JOURNAL OF MATERIALS SCIENCE 14(1979) 345–353

Fatigue crack initiation in Ti–6 wt % Al –4 wt % V castings

D. EYLON
Department of Materials Science and Metallurgical Engineering, University of Cincinnati, Cincinnati, OH 45221, USA

B. STROPE
Systems Research Laboratores, Inc., 2800 Indian Ripple Road, Dayton, OH 45440, USA

The lower ambient temperature fatigue life and higher fatigue data scatter of Ti–6 wt % Al–4 wt % V castings relative to wrought material, were investigated by analysing the nature of the crack initiation sites. Initiation mechanisms were characterized by precision sectioning the fracture surfaces at the crack nucleation locations. The combined effect of internal casting defects and a microstructure containing large colonies of similarly orientated α-platelets was found to be responsible for the low smooth fatigue life. The large scatter in the fatigue data was attributed to the variety of casting defects in the material and their large size distribution. Most failures that were examined initiated from defects close to the specimen surface possibly due to some bending moment in the axial cyclic loading. The free dendrite arms in the large shrinkage pores were shown to contain α-platelets in a colony arrangement. The shortest fatigue life associated with this type of defect was attributed to the notch effect of the dendrite arm interstices.

1. Introduction

Many Ti–6 wt % Al–4 wt % V alloy components are currently used in the aerospace industry and designed to operate in cyclically alternating stress conditions. The improvement of fatigue resistance is therefore a major goal in material and process development of this alloy [1–4]. Relatively inexpensive titanium alloy components can be provided by precision vacuum casting technology [5, 6], which eliminates most of the expensive machining costs. The tensile properties of the castings are comparable to the β-annealed wrought material, which has a similar microstructure. However, room temperature low [5] and high cycle [6] fatigue test results on the Ti–6 wt % Al–4 wt % V castings are inferior to wrought material results even when heat treated to the same condition. A large scatter of fatigue results is another characteristic of a cast alloy. Since the effective fatigue strength is restricted to the lower limit of the scatter band, this severely limits the design fatigue strength in castings.

It has been demonstrated in defect-free wrought Ti–6 wt % Al–4 wt % V with a variety of microstructures [4], that at the 10^6 cycle range, 99% of the fatigue life is spent in initiating a 0.5 mm crack. In the case of a β-annealed microstructure [7], rapid initiation or an existing internal flaw of this size caused a 95% fatigue life debit. An order of magnitude scatter in the fatigue results of a Ti–11 (6 wt % Al–2 wt % Sn–1.5 wt % Zr–1 Mo–0.35 wt % Bi) alloy with a β-annealed microstructure [8] was correlated with a large scatter in crack initiation behaviour.

The large number of defects that can be found in titanium alloy castings [5, 6], namely various types of porosity and inclusions, constitute potential sites for early crack nucleation. Therefore, a detailed investigation of the fatigue crack initiation mechanisms in cast Ti–6 wt % Al–4 wt % V is essential for the understanding of the lower fatigue life and the high scatter of the test

TABLE I Chemical composition of cast Ti–6 wt % Al–4 wt % V

Element	wt %
Al	6.2
V	4.1
Fe	0.16
C	0.02
H	0.0042
O	0.185
N	0.005
Ti	balance

results. An accurate characterization of failure origins can lead, through alloy and process modifications, to the elimination of those defects associated with the lowest fatigue lives and to a subsequent improvement in fatigue performance.

The investigation of the fatigue fracture origins in this work utilized a precision sectioning technique [7]. The sections through the initial crack locations revealed the underlying defects and microstructure and in some cases helped to determine the fatigue initiation mechanism.

2. Experimental

2.1. Material

The fatigue specimens analysed in this work were machined from cast Ti–6 wt % Al–4 wt % V components. The chemical composition of the cast material is given in Table I. An investment casting technique with wax patterns in a cluster assembly was used [6]. The alloy was melted and poured inside a skull crucible vacuum arc furnace. After the casting, the components were annealed for 2 hours at 720° C. The average room temperature tensile properties of the annealed defect-free material were: yield strength = 882 MNm^{-2}, ultimate tensile strength = 972 MNm^{-2}, elongation (in 4-D) = 8%, and reduction of area = 15%.

2.2. Microstructure and defects

The cast and annealed microstructure shown in Fig. 1a is an α-platelet structure arranged in either basketweave (A) or colony (B) morphology of similarly aligned and crystallographically orientated platelets formed on transformation from the β-phase region. Long α-phase platelets outline the boundaries of the prior β-grains (C) and therefore are named grain-boundary alpha. With slow cooling rates the material will tend to develop a colony rather than a basketweave structure; therefore, the α-platelet morphology depends upon the location within the casting.

Three major types of porosity defects were identified in the cast material. The first one is gas-induced porosity. An example of this is shown in Fig. 1a D. The pores are spherical in shape and range in diameter from 0.02 to 1 mm. The second type is small shrinkage porosity like E in Fig.1a. These have indefinite shapes and range in size from 0.005 to 0.02 mm. The third type are large

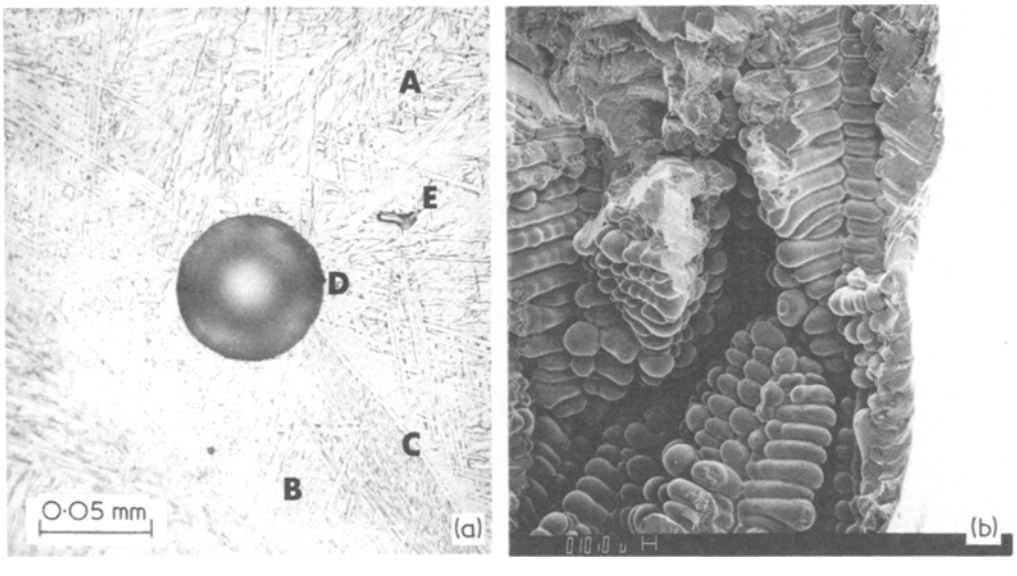

Figure 1 (a) Basketweave (A), colony (B) and grain-boundary α-phase (C) morphology in Ti-6 wt % Al-4 wt % V castings containing gas-induced pore (D) and small shrinkage pore (E). (b) Large shrinkage dendritic pore.

TABLE II High cycle room temperature axial fatigue tests, $R = 0.1$ [6]

Specimen number	Maximum cyclic stress ($MN\,m^{-2}$)	Cycles to failure (N_f)	Specimens analysed in detail	Initiation defect
1	414	8.5×10^4	X	gas pore
2	414	9.7×10^4	X	small shrinkage pore
3	414	5.7×10^4		large dendritic pore
4	414	2.3×10^5	X	α-platelets colony
7	414	5.0×10^4	X	large dendritic pore
15	414	1.2×10^5		small shrinkage pore
16	414	8.6×10^4		gas pore
18	414	1.0×10^5		small gas pore

shrinkage pores like the one shown in the SEM image in Fig. 1b. In poor castings these pores could reach 6 mm in size. Material solidified on their surface in a free dendritic formation. As will be discussed later in the precision sectioning analysis, the dendritic arms transform into colonies of α-platelets during the cooling from the β-phase, which will be used to explain their cleavage-like fracturing.

2.3. Fatigue tests

To enable positive identification of the initiation sites in the cast material, only specimens tested in axial fatigue with $R > 0$ were selected for analysis ($R = \sigma_{min}/\sigma_{max}$). Since these specimens were loaded in a tension/tension mode, the fracture surfaces were not damaged during fatigue cycling and it was possible to identify the exact crack initiation site. The use of smooth axial fatigue specimens increased the probability of obtaining substructure crack initiation at material defects rather than on the specimen surface [9]. Flat smooth fatigue specimens with 10 mm × 2.5 mm gauge section and 25 mm gauge length were used. The high cycle fatigue specimens were tested at room temperature, 1800 cycles min^{-1}, and $R = 0.1$ [6].

To make valid comparisons among the different samples, four fatigue specimens out of a group of eight (Table II), all tested at the same stress level, were selected for detailed analysis. Fig. 2 shows the relative location of each specimen with-

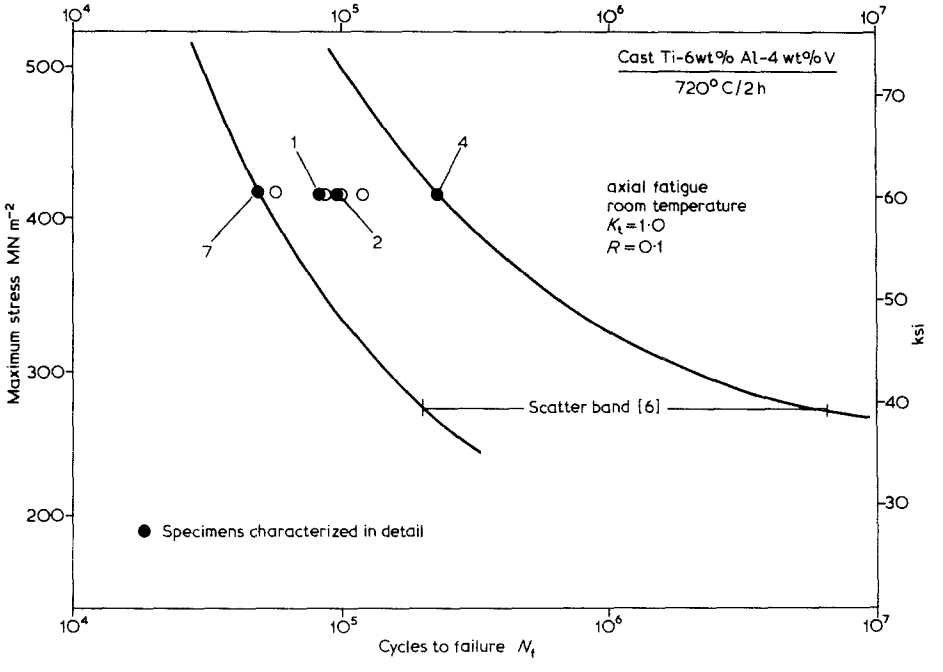

Figure 2 S–N curve for Ti–6 wt % Al–4 wt % V castings with a wide scatter band. Specimens 1, 2, 4, and 7 were used for detailed crack initiation analysis.

in the scatter band to allow correlation of the fatigue results with the type of defects responsible for the crack initiation.

2.4. Fractography and precision sectioning

The fatigue crack initiation sites were identified by scanning electron microscopy performed on an ETEC scanning electron microprobe. After locating the sites, the specimens were sectioned perpendicular to the fracture surface through the initiation site. This precision sectioning technique is described in detail elsewhere [7]. The sectioned surface was polished and etched with Kroll's reagent and photomicrographs of the initiation location and the underlying microstructure were taken. After the optical examination the mounting material was dissolved. It was then possible to obtain a combined micrographic/fractographic image of the fracture surface and the initiation site.

3. Crack initiation analysis

3.1. Dendritic pore initiation

Examination of Specimen 7, which represents the lower fatigue life value of the scatter band in

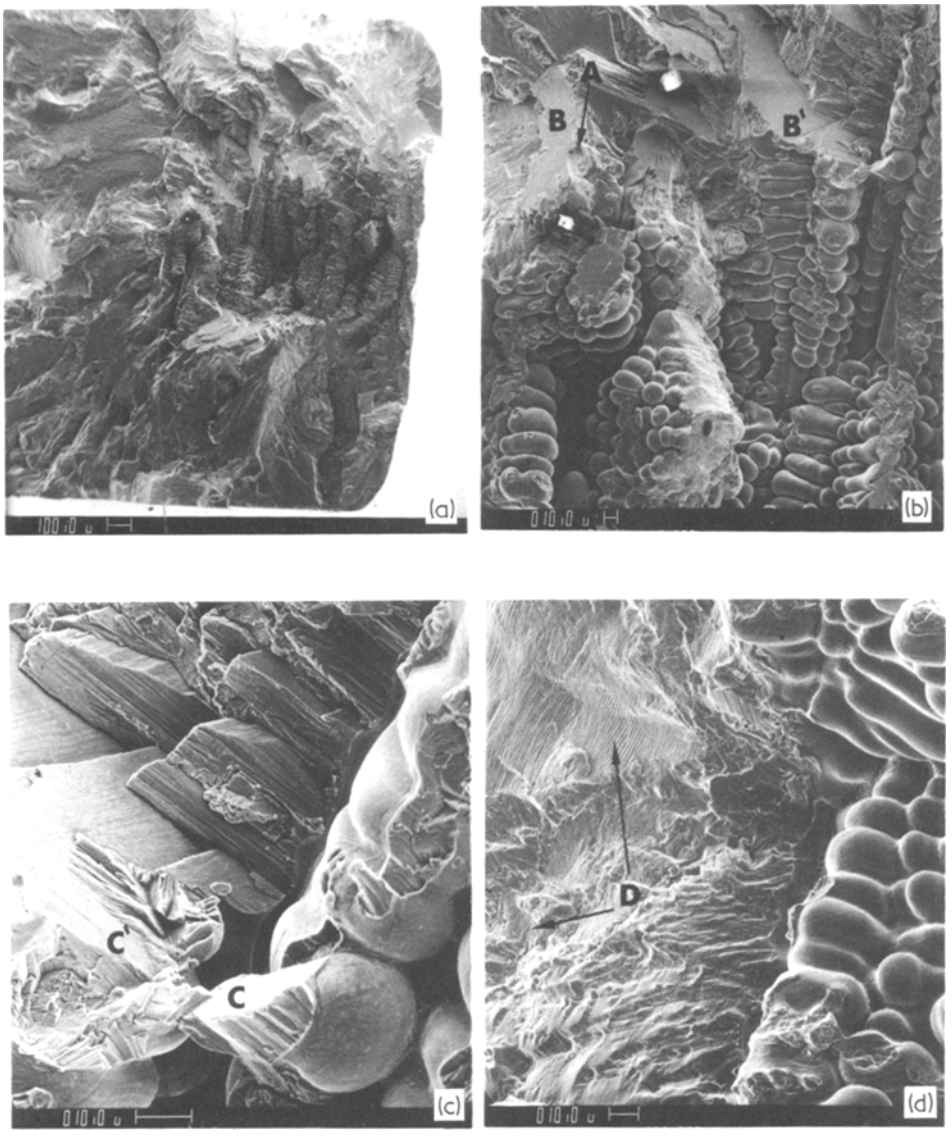

Figure 3 Fatigue crack initiation at large shrinkage dendritic pore of Specimen 7: (a) A general view; (b) Initiation at A, cleavage-like fracture facets at B and B′; (c) Dendrite arm cleavage-like fracture at C and C′; (d) Ductile fatigue striations at D.

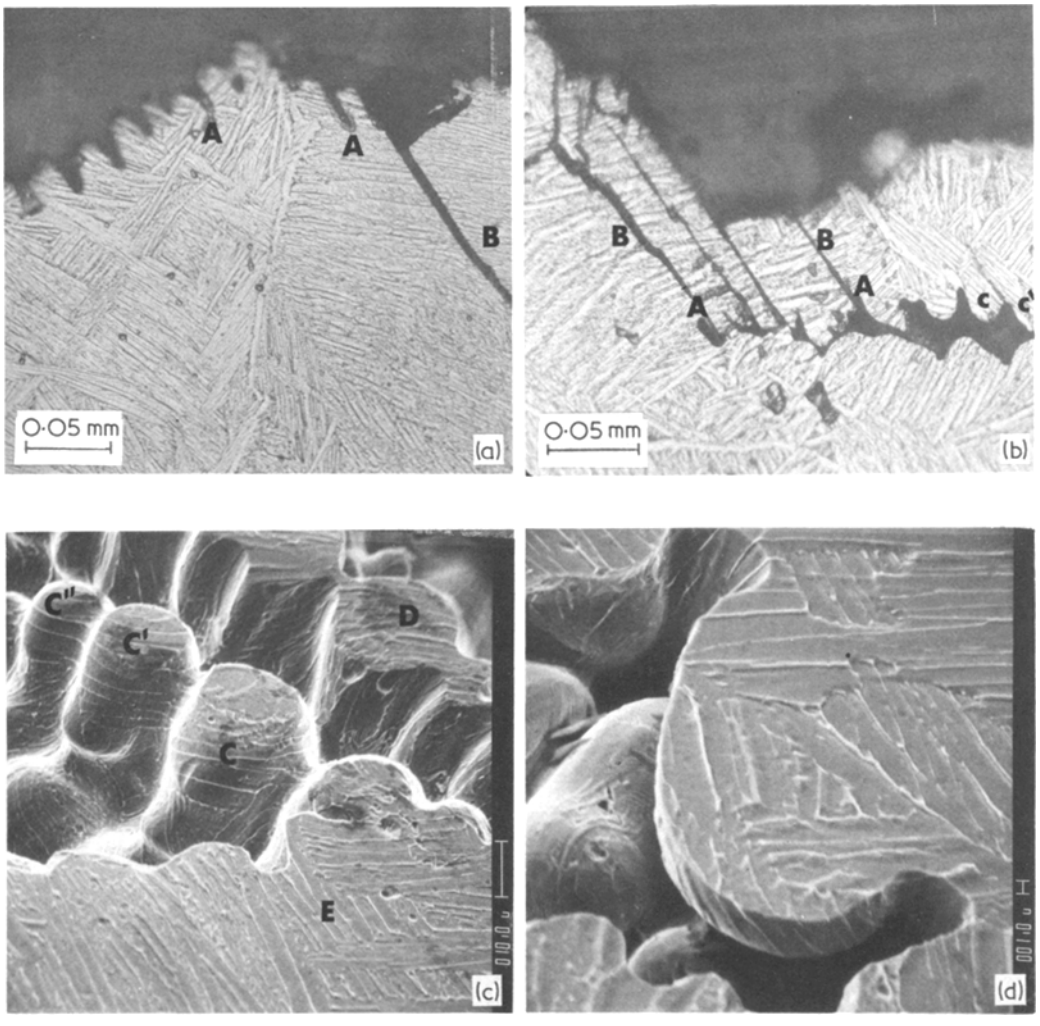

Figure 4 Section through the initiation site of Specimen 7: (a) Crack initiation at dendrite interstices (A), and shear related propagation across a colony (B); (b) Crack initiation (A), parallel cracking (B), dendrites with common orientation (C and C′); (c) Common orientation on the etched surface of dendrites (C, C′ and C″) and dendrite cleavage-like fracture at D. The microstructure is shown on the polished and etched surface E of the sectioned specimen; (d) Section through dendrite with several α-platelet orientations.

Fig. 2, revealed crack initiation at a large dendritic shrinkage pore (1.2 mm length) located close to the specimen surface (Fig. 3a). A fatigue crack initiation site can be seen in Fig. 3b at A. The crack propagated from right to left on the cleavage-like facet B. Another cleavage-like facet is shown at B′. A higher magnification fractograph in Fig. 3c shows that the dendrite arms can also fatigue fracture in a cleavage-like mode (C and C′). However, when the crack propagates away from the initiation zone (Fig. 3d), ductile fatigue fracture, manifested by fatigued striations (D), can take place.

Cleavage-like fatigue fracture facets are frequently found in β-annealed microstructures of $(\alpha + \beta)$ titanium alloys with large α-platelet colonies [10–14], similar to the cast microstructure shown in Fig. 1a. The fatigue facets were found to be related to intense shear across the whole colony in a direction perpendicular or at an angle to the long axis of the α-platelets. This shear related fracture can initiate at the specimen surface [7] (Ti–6 wt % Al–4 wt % V), at some subsurface defect [11, 12] (IMI-685), or subsurface at a large colony of α-platelets with no apparent defect [14] (Ti–6 wt % Al–4 wt % V).

To identify the nature of the crack initiation facets, these locations were precision sectioned. The micrographs in Figs. 4a and 4b show the microstructure below the dendrite arms at the

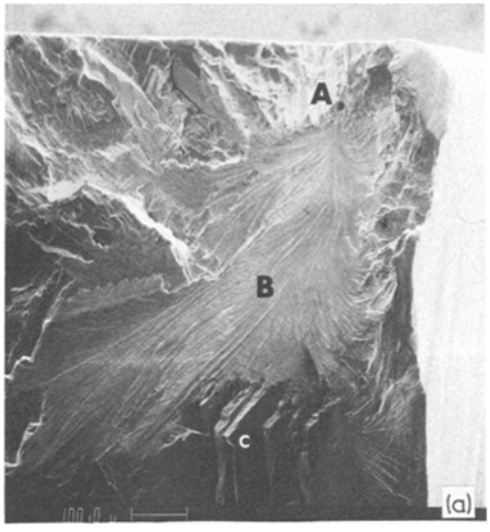

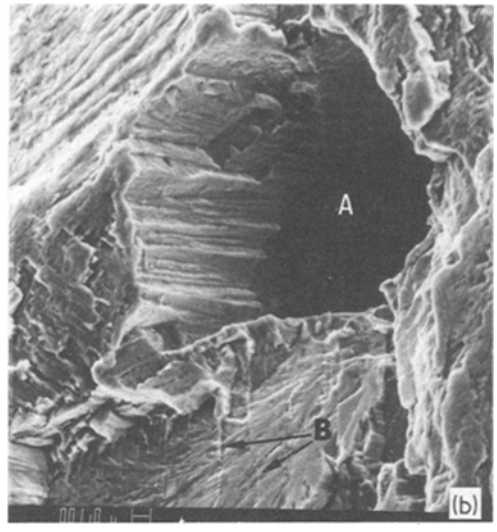

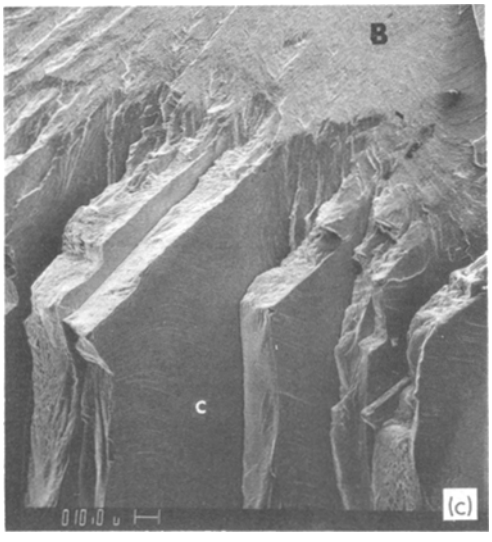

Figure 5 Small shrinkage pore initiation in Specimen 2: (a) A general view; pore (A), cleavage-like fracture (B); (b) Pore (A) and α/β interfaces (B) on fracture surface; (c) Step facets (C).

cleavage-like fracture areas shown in Figs. 3b and 3c. It can be seen that the cracks initiated at the dendrite arm interstices (A). The long, planar, shear-related cracks extend across large colonies in a manner similar to the fatigue cracks described in [10–12]. The microstructure of the dendrite arms is also a colony-type structure as a result of cooling through the $(\alpha + \beta)$ phase region during the casting. In some cases (Fig. 4b) one or more arms (C and C′) and the area behind them belong to the same colony. This makes the intensive shear activity very easy since the arm interstices (which act as stress risers) and the adjacent material have the same crystallographic orientation [11]. The fracture surface in Fig. 4c was lightly etched to remove the vapour deposition patterns and reveal the microstructure. The α-platelets morphology shows that C, C′ and C″ have the same orientation and probably belong to the same colony. The planar fracture of a free dendrite arm can be seen at D. The microstructure of the polished and etched section plane is shown at E. Unlike the dendrites shown in Figs. 4b and 4c, the higher magnification photomicrograph of a section through another dendrite in Fig. 4d shows several orientations of α-platelets within one arm.

The fact that the fatigue life of this specimen was the lowest of the group studied is therefore attributed to the large dendritic pore which provided several fatigue crack initiation sites. Dendrite interstices within the colony structure may also have enhanced the intense shear activity leading to earlier crack initiation.

3.2. Small shrinkage pore initiation

Crack initiation at a small shrinkage pore located close to the specimen surface was observed in Specimen 2 (Table II). This specimen had a medium fatigue life within the data scatter band (Fig. 2). A pore (A in Fig. 5a) initiated a cleavage-like fracture at B. A higher magnification fractograph of A is shown in Fig. 5b. The platelet structure of the cleavage-like propagation facet (B) can also be seen in this figure. The large step-like facets (C) in Fig. 5c are typical of parallel slip/fracture activity like that shown in Fig. 4b.

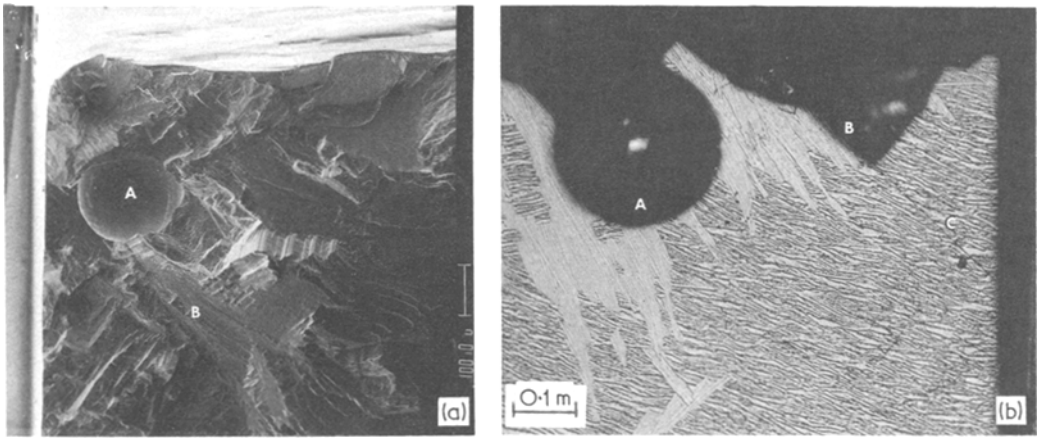

Figure 6 (a) Gas pore initiation in Specimen 1, with pore (A) and cleavage-like initiation (B); (b) Section through the initiation site, showing also shear extending into the colony structure at C.

This type of fatigue fracture will normally occur in large colonies which are favourably orientated with respect to the major tension axis for easy slip [15].

3.3. Gas pore initiation

In Specimen 1 (Table II), which represents medium fatigue life, gas pore initiation was observed. As in the previously examined specimens, the crack-initiating defect was located close to the specimen surface (Fig. 6a, A) and the cleavage-like facets (B) emanating from it. The section in Fig. 6b was made through A and B in Fig. 6a. The shear related fracture facet B, has extended at C into the large colony of α-platelets underlying the gas pore.

3.4. Large colony shear initiation

Specimen 4, with the highest fatigue life in the scatter band (Fig. 2), did not show defect-related initiation. Although some defects were present at the fracture surface (dendritic pore at A′ and gas pore at A″ in Fig. 7a), they were not near the specimen surface and the fatigue crack initiated from the flat facet at A. The higher magnification fractograph in Fig. 7b shows the crack initiation region at A and the propagation region at B. The section through A and B along line C (Fig. 7c), shows that the crack initiated in a shear-related mode within colony A and propagated into colony B. The colonies in this region are very large, almost the size of the prior β-grains outlined by grain boundary alpha.

4. Discussion

4.1. Crack initiation location

It is significant that of the many defects observed on the fracture surfaces, all the pore-related failures initiated from a defect located close to the specimen surface. Similar near-surface fatigue crack initiation was previously observed in titanium alloy [16] and superalloy [9] powder compacts containing nonmetallic inclusions and porosity. Since most axial fatigue test equipment is misaligned to a certain degree, bending moments will develop during the loading cycle. As a result, some locations at the specimen surface will develop higher tensile stresses. Defects nearest to this maximum stress location will have a higher probability of initiating fatigue cracks. Therefore, sometimes a relatively small defect near the surface (as in Specimen 2) will initiate a crack even though larger defects may exist within the material. It is the nature of this defect at the maximum stress location that determines the fatigue life of the test specimen. Near-surface defect crack initiation is common in fatigue service failures, since most components are loaded in a mixed mode of axial loading and bending.

4.2. Crack initiation mechanism

It appears that in the Ti–6 wt % Al–4 wt % V castings, crack initiation is influenced by a combination of defects and microstructure. The pores act like stress risers to increase local stresses and the shear susceptible colony microstructure [11, 14] increases the chance of early initiation. The

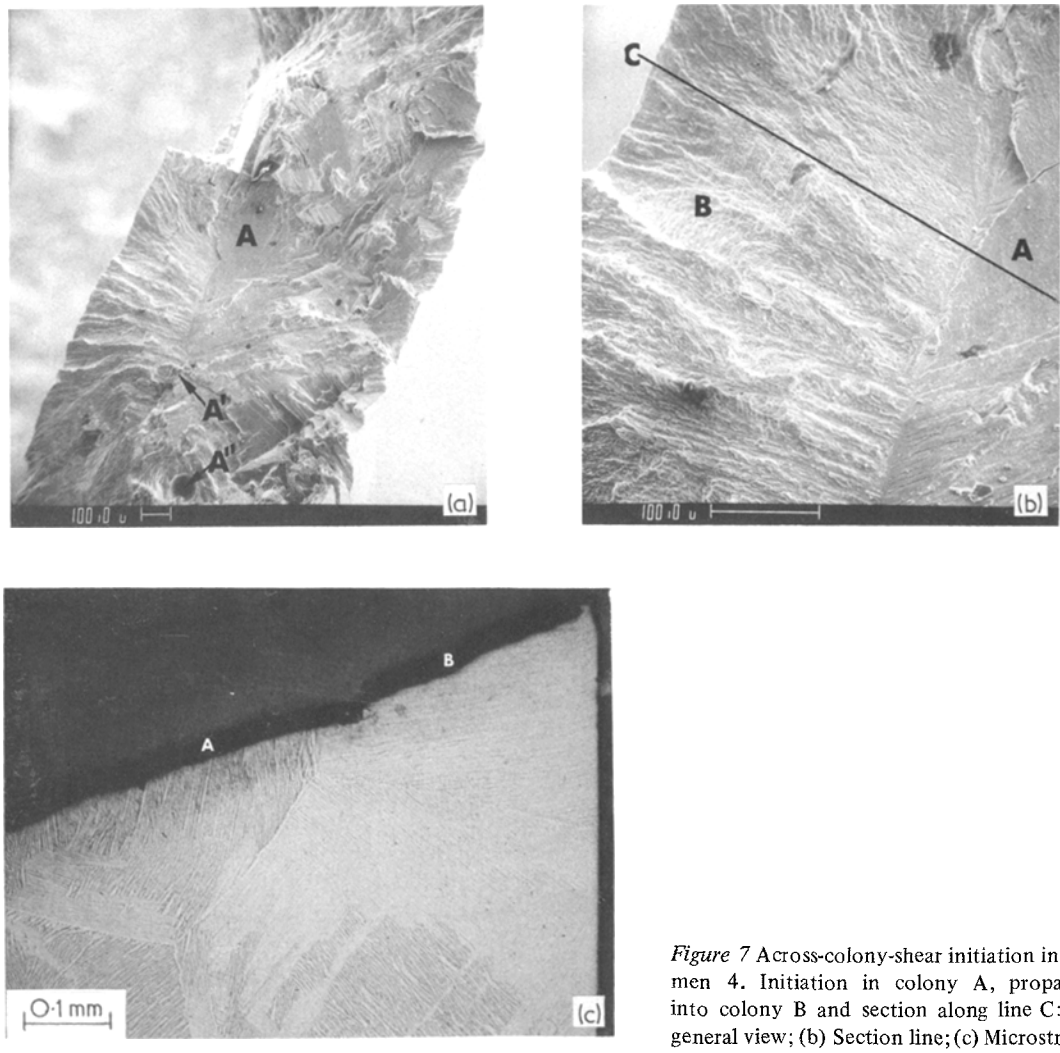

Figure 7 Across-colony-shear initiation in Specimen 4. Initiation in colony A, propagation into colony B and section along line C: (a) A general view; (b) Section line; (c) Microstructure under the initiation site along line C.

internal pores enhance intense shear by accommodating subsurface slip and by increasing stresses at certain locations. In Specimen 4 the fatigue crack initiated by shearing across a large colony. Even though it has the highest life in the scatter band, the fatigue strength was lower than β-processed wrought material, which typically has smaller colonies [17]. Lower life was also attributed to initiation in large colonies in notch [7] and low cycle fatigue [14] of wrought β-annealed Ti–6 wt % Al–4 wt % V.

4.3. Data scatter and defects

Although the number of specimens used was too small for correlation of defect initiation with scatter band data, some observations can be made. Large dendritic pore initiation was associated with the lowest fatigue life of the specimens examined. This may be due to its relatively large size, and also to the dendrite arm interstices which provided sharp notch crack initiation sites.

Small shrinkage pore and the gas pore initiation corresponded to medium fatigue life. Although some of the gas pores were larger in size than the small shrinkage pores, their spherical shape reduces their effectiveness as stress risers.

Across-colony-shear initiation was associated with the best fatigue life in the group although the fatigue life was still lower than defect-free wrought material with a smaller colony size.

5. Conclusions

The following conclusions were reached:

(a) The lower fatigue strength of cast

Ti–6 wt % Al–4 wt % V relative to wrought material is attributed both to the existence of internal defects and a shear sensitive microstructure of colonies of similarly orientated α-platelets, enhancing early crack initiation.

(b) Large dendritic shrinkage pores, small shrinkage pores and gas pores are the main defects existing in the castings examined.

(c) Variations in the nature of the porosity and pore sizes are responsible for the large scatter in the fatigue results.

(d) Dendritic pore initiation was associated with the lowest fatigue life and the across-colony-shear with the highest fatigue results.

(e) Cracks were initiated at defects close to the specimen surface possibly due to bending moments existing in the fatigue load cycle.

Acknowledgements

The authors wish to acknowledge Mr K. Love of the Manufacturing Technology Division, Air Force Materials Laboratory, for his support of this work, and also to Mr M. M. Allen and W. T. Barice of Pratt and Whitney Aircraft Group and Mr W. Grant of Grumman Aerospace Corporation for providing the material for this work. Mr W. A. Houston of the University of Cincinnati is acknowledged for his metallographic assistance. The helpful comments of Dr L. R. Bidwell and Dr T. L. Bartel of the Air Force Materials Laboratory are highly appreciated. This work is part of a combined research effort by the University of Cincinnati, the Systems Research Laboratories and the Air Force Materials Laboratory.

References

1. R. A. SPRAGUE, D. L. RUCKLE and M. P. SMITH, "Titanium Science and Technology", Vol 3, edited by R. I. Jaffee and H. M. Burte, (Plenum Press, New York, 1973) p. 2069.
2. J. J. LUCAS, *ibid.* p. 2081.
3. A. W. BOWEN and C. A. STUBBINGTON, *ibid.* p. 2097.
4. D. EYLON and C. M. PIERCE, *Met. Trans. A,* 7A (1976) 111.
5. V. L. HELLMANN and T. C. TSARETT, Air Force Materials Laboratory Report: AFML-TR-71-47, July 1971.
6. M. M. ALLEN, W. J. BARICE and W. GRANT, Air Force Materials Laboratory Report: AFML-TR-76-192.
7. W. R. KERR, D. EYLON and J. A. HALL, *Met. Trans A* 7A (1976) 1477.
8. D. EYLON and W. R. KERR, "Fractographic Approach to Failure Analysis", ASTM STP 645 (American Society for Testing and Materials, Philadelphia, 1978) p. 235.
9. D. EYLON and J. M. HYZAK, *Met. Trans. A* 9A (1978) 127.
10. D. EYLON, J. A. HALL, C. M. PIERCE and R. L. RUCKLE, *ibid.* 7A (1976) 1817.
11. D. EYLON and J. A. HALL, *ibid.* 8A (1977) 981.
12. D. EYLON, *Microscope* 23 (1975) 133.
13. G. R. YODER, L. A. COOLEY and T. W. CROOKER, *Met. Trans. A* 8A (1977) 1737.
14. J. RUPPEN, P. BHOWAL, D. EYLON and A. J. McEVILY, *ASTM STP,* in press.
15. D. EYLON and P. J. BANIA, *Met. Trans.* 9A (1978) 1273.
16. D. EYLON and N. BIRLA, *ibid.* 8A (1977) 367.
17. F. L. PARKINSON, The Boeing Company Report No. FAA-SS-72-00, July 1972.

Received 13 March and accepted 1 June 1978.